Synthesis of a Porous, Biocompatible Tissue Engineering Scaffold Selectively Degraded by Cell-Generated Reactive Oxygen Species

By

John Robert Martin

Thesis

Submitted to the Faculty of the

Graduate School of Vanderbilt University

in partial fulfillment of the requirements

for the degree of

MASTER OF SCIENCE

In

Biomedical Engineering

December, 2013

Nashville, Tennessee

Approved:

Craig L. Duvall, Ph.D.

Scott A. Guelcher, Ph.D.

To my parents, Rob and Katie, for giving my every opportunity to succeed in life and supporting me

every step of the way

and my sisters, Ginny and Emily, for their boundless love and support.

ACKNOWLEDGEMENTS

TABLE OF CONTENTS

LIST OF FIGURES

LIST OF TABLES

CHAPTER I

INTRODUCTION

Bone Defect Repair

Every year, roughly two million patients worldwide undergo a bone grafting procedure to repair a

bone defect caused by trauma, congenital defects, tumor excision, or disease[1]. The gold standard

treatment is to harvest the bone graft from an autologous source on the patient's iliac crest, though the

required second surgery and harvest-site morbidity concerns[2] make this treatment method problematic.

The use of allograft bone has also been explored for treating bone defects, though potential negative

patient immunologic responses from these materials can limit their effectiveness. Therefore, much

effort has been devoted to developing tunable synthetic materials that promote bone regrowth but are

safely tolerated by the patient's body. Implantable devices made with poly(methyl methacrylate)

(PMMA) have been clinically used for bone replacement/fixation owing to their robust mechanical

properties which can closely mimic those of native bone tissue[3]. However, PMMA cannot be resorbed

by the body and can induce an inflammatory response[4]. Injectable calcium phosphate (CaP) bone

cements have shown promise as a synthetic bone graft substitute, though treatment effectiveness has

been limited by mismatches between rate of CaP degradation and the rate of new tissue growth[5].

Thus, there exists a substantial need for biomaterials that foster new bone tissue growth, exhibit

biocompatibility in both the bulk material and the degradation byproducts, provide mechanical stability

at the wound site, and effectively match the rate of new tissue growth with the rate of material

biodegradation.

Poly(ester-urethane) Tissue Engineering Scaffolds

Biodegradable scaffolds made from synthetic polymers have been extensively investigated for

use in tissue engineering and regenerative medicine, including bone defect repair applications.

Examples include poly(lactic-*co*-glycolic acid) (PLGA) [6, 7], poly(ε-caprolactone) (PCL) [8, 9], polyanhydrides (PAA) [10, 11], and polyurethanes [12, 13], all of which have a history of use in products approved by the FDA [14-17]. These materials are applicable for a diverse range of regenerative applications because they offer a high degree of tunability, generate a minimal host inflammatory response, and degrade into non-cytotoxic components [18, 19] that are resorbed and cleared from the body [20, 21].

In situ curing, injectable scaffolds such as poly(ester urethanes) (PEURs) that support cellular infiltration and degrade into non-toxic breakdown products represent a particularly promising class of biomaterial [22]. Porous PEUR scaffolds are formed by mixing hydroxyl-functionalized polyols (*e.g.*, 900 g mol^{-1} triols comprised of caprolactone, glycolide, and D,L-lactide) [18] with isocyanate-functional precursors to form a crosslinked network. Water can be added as a blowing agent to create an inter-connected pore structure, and the mechanical, chemical, and degradation properties of the scaffold can be modified through the selection of the polyol and isocyanate precursors [23, 24]. Unlike many other techniques used for fabrication of porous scaffolds, this approach does not require a porogen leaching step. This *in situ* foaming method, combined with the relatively short working time of the reactive liquid mixture [25], renders PEURs useful as injectable and settable scaffolds suitable for minimally invasive procedures in the clinic for the repair of bone defects.

PEUR scaffolds are primarily degraded by acid-catalyzed hydrolysis of ester bonds in the amorphous soft segment, resulting in chain scission and formation of hydroxyl and carboxylic acid end groups. Residual carboxylic acids in the polymer reduce the local pH at later stages of degradation [26, 27], thereby catalyzing accelerated hydrolysis of the polymer [28]. As the polymers degrade, low molecular weight and soluble α-hydroxy acids diffuse from the scaffold into the medium, resulting in mass loss. Although α-hydroxy acids are non-toxic and can be cleared from the body [18, 29], autocatalytic degradation of the PEUR network driven by residual carboxylic acid groups can result in a mismatch in the rates of scaffold degradation and tissue in-growth that leads to resorption gaps and compromised tissue regeneration [30].

Approach

To overcome the autocatalytic degradation behavior exhibited in polyester-based bone tissue engineering scaffolds, we propose to utilize scaffold materials whose degradation is exclusively tied to cellular activity. In particular, biomaterials that degrade by cell-mediated mechanisms, such as materials with protease-cleavable peptides, have been successfully utilized to synthesize environmentally-sensitive nanoparticles [31, 32], hydrogels [33, 34], and polymeric scaffolds [35, 36]. However, it is difficult to establish this approach as a generalizable tissue engineering platform because these peptide sequences are cleaved by specific enzymes that are upregulated in specific pathological environments [37] and feature highly variable levels across patient populations [38]. Also, manufacturing peptides on the scale necessary to fabricate large tissue scaffolds is both expensive and time-consuming with current technology [39]. Development of degradable polymers that can be affordably synthesized in large scales, similar to polyesters, but that target a ubiquitous cell-mediated signal for scaffold degradation may provide a more generalizable and better-performing biomaterial. Scaffolds degraded by cell-generated reactive oxygen species (ROS) are a promising candidate because ROS serve as important biological mediators in many normal biological processes [40], and elevated ROS, or "oxidative stress", is a hallmark of inflammation and the pathogenesis of myriad diseases [41]. Polymeric biomaterial implants have also been shown to elicit a stable three-fold increase in ROS production at surgery sites over a four week timeframe [42], further highlighting the potential utility of this cell-generated signal for triggering material degradation. This has motivated the recent emergence of new classes of ROS-responsive polymer-based nanoparticles [43-48] and development of salt-leached, porous scaffolds composed of a combination of the polyester PCL and ROS-sensitive, proline-based peptides [49].

Here we sought to develop a generalizable, cell-degradable polyurethane scaffold formulated from polyols exhibiting ROS-dependent degradation. To do so, we synthesized a new class of polyols based on ROS-degradable poly(thioketals) which are stable under aqueous conditions but are selectively degraded by cell-generated ROS. These fully synthetic, non-peptide based scaffolds have been developed to further explore utilization of an ROS-dependent degradation mechanism in order to

3

yield scaffolds with better matched rates of cellular infiltration and degradation to enhance repair of

bone tissue defects (see **Figure 1)**.
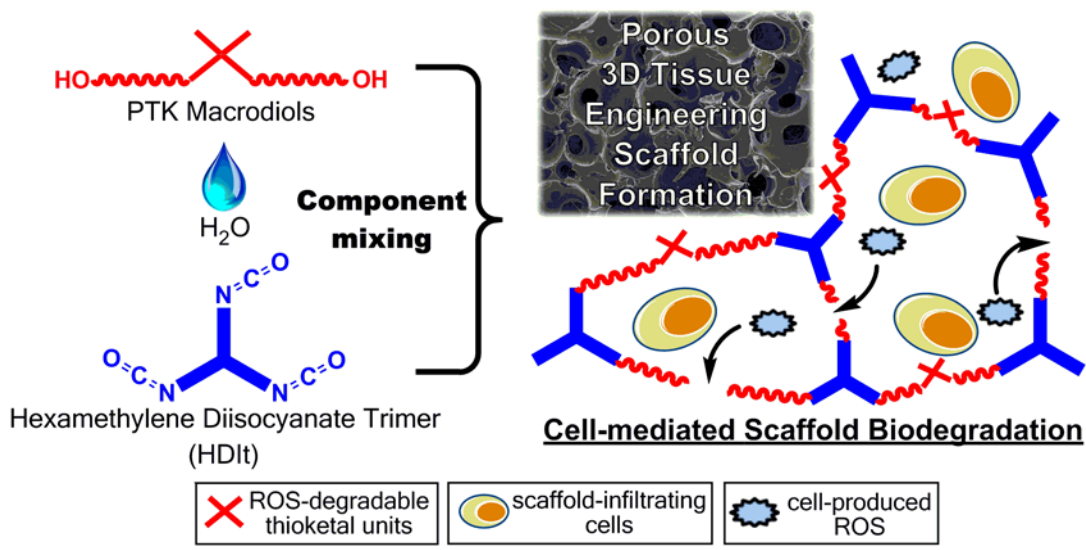
Figure 1. Scheme for the formation of ROS-degradable tissue engineering scaffolds. The reaction between hydroxyl-functionalized PTK polymers, water, and a tri-functional isocyanate yields porous 3D scaffolds that are selectively degraded by cell-produced ROS.

CHAPTER II

SYNTHESIS OF A POROUS, BIOCOMPATIBLE TISSUE ENGINEERING SCAFFOLD SELECTIVELY
DEGRADED BY CELL-GENERATED REACTIVE OXYGEN SPECIES

Introduction

Synthetic polyester-based tissue engineering scaffolds represent a promising biomaterial therapy for the treatment of bone defects. In particular, *in situ* curing, injectable PEUR scaffolds have been shown to help mediate the regeneration of bone tissue in critically-sized defects[25, 30, 50]. PEURs are primarily degraded by hydrolysis, though the scission of ester bonds in the polymer chains generates acidic byproducts which catalyze further hydrolysis. This autocatalytic behavior can result in a mismatch in the rates of scaffold degradation and tissue in-growth that leads to resorption gaps and compromised tissue regeneration [30]. To overcome this late-stage scaffold failure, materials that are degraded solely by cell-mediated activities have been developed. Rather than utilizing scaffolds comprised of synthetic peptides that are selectively cleaved by cell-generated enzymes[33, 36], the most common methodology for achieving cell-mediated degradation, ROS-degradable scaffolds were developed. Nearly all the ROS-degradable materials reported to date have been applied in nanoparticles, with an oligo-proline peptide-based scaffold being the only currently developed ROS-degradable tissue engineering material[49]. This approach for achieving scaffold biodegradation takes advantage of the body's natural ROS production and is predicted to yield materials that are both more cost-efficient than peptide-based scaffolds while possessing a more controlled degradation profile.

In the current study, we synthesized a new class of polyols based on ROS-degradable poly(thioketals) which are stable under aqueous conditions but are sensitive to oxidation. Poly(thioketals) (PTKs) were recently applied for development of orally-delivered nanoparticles that remain stable in transit through the stomach and specifically release their cargo "on demand" at sites of ulcerative colitis[44]. To date, however, this unique polymer chemistry has solely been utilized in targeted nanoparticle drug delivery applications[44, 48]. Herein, we report the development and testing of a new

5

class of PTK macrodiols amenable to synthesis of injectable, porous poly(thioketal)-urethane (PTK-UR) tissue engineering scaffolds that are selectively degraded by cell-generated ROS. These fully synthetic, non-peptide based scaffolds have been developed to further explore utilization of an ROS-dependent degradation mechanism in order to yield scaffolds with better matched rates of cellular infiltration and degradation to enhance repair of bone tissue defects.

Methods

Materials

All chemicals were purchased from Sigma-Aldrich (Milwaukee, WI, USA) except the following. 2-mercaptoethyl ether (MEE), glutaraldehyde, and cobalt chloride were purchased from Fisher Scientific (Pittsburgh, PA), and the tertiary amine catalyst (TEGOAMIN33) was obtained from Goldschmidt (Hopewell, VA). Glycolide and D,L-lactide were obtained from Polysciences (Warrington, PA). Coscat83, an organobismuth urethane catalyst, was supplied by ChasChem, Inc. (Rutherford, NJ). Hexamethylene diisocyanate trimer (HDIt, Desmodur N3300A) was received as a gift from Bayer Material Science (Pittsburgh, PA). Cell culture reagents, including Dulbecco's Modified Eagle Medium (DMEM), fetal bovine serum (FBS), and penicillin/streptomycin were supplied by Gibco Cell Culture (Carlsbad, CA). All materials were used as received unless otherwise indicated.

PTK Dithiol Synthesis

The condensation polymerization protocol for PTK prepolymer synthesis was adapted from Wilson et al.[44]. Briefly, p-toluenesulphonic acid monohydrate (PTSA) was added to a tri-necked boiling flask equipped with an attached addition funnel. The vessels were placed under vacuum for 15 min before being purged with nitrogen. The boiling flask was charged with anhydrous acetonitrile and batch-specific amounts of MEE (x molar eq) and 1,4 butanedithiol (BDT) (1-x molar eq) where x = 1, 0.75, 0.5, 0.25, and 0 for the synthesized PTKs, respectively. The addition funnel was also charged with

6

anhydrous acetonitrile and 2,2-dimethoxypropane (DMP) (0.83 molar eq). A molar excess of dithiol monomers was utilized relative to DMP to ensure the formation of polymers with free terminal thiols. Both the addition funnel and boiling flask's solutions were purged with flowing nitrogen for 30 min before submerging the boiling flask into an oil bath at 80°C. After 15 min of temperature equilibration, the addition funnel stopcock was set so that the acetonitrile-DMP solution was added drop-wise into the continuously stirring boiling flask over a period of 16 h. Post synthesis, the acetonitrile was removed by rotary evaporation and the resultant PTKs were isolated by precipitation into cold ethanol and dried under vacuum. To evaluate polymer compositions, samples of the respective PTKs were dissolved in deuterated chloroform (CDCl$_3$) and analyzed with ^{1}H nuclear magnetic resonance spectroscopy (NMR, Bruker 400 MHz Spectrometer). ^{1}H NMR chemical shifts were reported as δ values in ppm relative to the deuterated CDCl$_3$ (δ = 7.26). Multiplicities are reported as follows: s (singlet), d (doublet), t (triplet), and m (multiplet). The number of protons (n) for a given resonance is indicated as nH and is based on integration values. ^{1}H NMR (400 MHz, CDCl$_3$): δ = 3.67-3.61 (m, 4H), δ = 2.83 (t, 4H), δ = 2.63 (t, 4H), δ = 1.72 (t, 4H), δ = 1.60 (s, 6H).

Polyester Polyol Synthesis

Trifunctional or bifunctional polyester polyols were synthesized as previously documented[18]. To synthesize the trifunctional polyol, glycerol was vacuum dried for 48 h at 80°C and then added to a 100 mL three neck flask. By molar amount, 60% ε-caprolactone, 30% glycolide, and 10% D,L-lactide were added to the glycerol starter along with a stannous octoate catalyst to yield a 900 g mol^{-1} triol, a 1000 g mol^{-1} diol, and a 1500 g mol^{-1} triol.

PTK Hydroxyl Functionalization

The hydroxyl-functionalization of the PTK dithiols was completed[51] in order to generate polyols compatible with standard polyurethane synthesis. Briefly, PTK dithiol polymers were transferred to a boiling flask, placed under vacuum, and then exposed to a nitrogen atmosphere. The flask was charged

with anhydrous dichloromethane (DCM) before adding a 10x molar excess of β-mercaptoethanol to the solution. This solution was stirred continuously at room temperature to reduce any disulfide bonds and recover the reactive thiol end groups. After 3 h of stirring, the DCM was evaporated and the residue was washed three times in cold ethanol to remove residual β-mercaptoethanol. The reduced PTK polymers were dissolved in anhydrous tetrahydrofuran (THF) before adding a 10x molar excess of cesium carbonate ($CsCO_3$) under nitrogen and stirring for 30 min at room temperature. A 5x molar excess of 2-bromoethanol was next added to the solution and stirred for 18 hours under nitrogen at room temperature. After stirring, the solution was added to a separation funnel with an excess of deionized water to effectively separate the PTK-solubilizing THF layer from the water-soluble $CsCO_3$ catalyst. The hydroxyl-functionalized PTKs were extracted in THF before removing the solvent by rotary evaporation, followed by precipitation three times in cold ethanol before vacuum drying for 24 h. Molecular weights and polydispersities of the five synthesized PTK diols were analyzed by gel permeation chromatography (GPC, Agilent Technologies, Santa Clara, CA) using a mobile phase of *N,N*-dimethylformamide (DMF) with 100mM LiBr. Polymer molecular weights were quantified using a calibration curve generated from poly(ethylene glycol) (PEG) standards (400 – 4000 g mol^{-1}). Hydroxyl-functionalization was confirmed by ^{1}H NMR (400 MHz, $CDCl_3$): δ = 2.74 (t, 4H) and attenuated total reflectance Fourier transform infrared spectroscopy (ATR-FTIR; Bruker Tensor 27 FTIR, Billerica, MA). For ATR-FTIR, thiol-terminated and hydroxyl-terminated PTK polymers were placed in contact with a ZnSe ATR crystal to quantify absorbance at 2550 cm^{-1} and 3400 cm^{-1}, which correspond to absorbance peaks of free thiol and free hydroxyl groups, respectively. The hydroxyl (OH) numbers of the different PTK diols were determined by titration (Metrohm 798 MPT Titrino, Herisan, Switzerland) according to ASTM E1899 – 08 [52]. **Eq (1)** was used to relate the molecular weight to the hydroxyl number of each titrated PTK:

$$M_n = \frac{56100f}{OH\ number} \tag{1}$$

where 56,100 represents the molecular weight of KOH in mg/mol, f represents the hydroxyl functionality of the PTK (assumed to be 2 for the linear homobifunctional polymers in this study), and M_n represents the number-average molecular weight of the polymer.

PTK-UR and PEUR Synthesis

The PTK-UR and PEUR scaffolds were prepared using two-component reactive liquid molding of: (a) hexamethylene diisocyanate trimer (HDIt), and (b) a hardener component comprising the PTK diol, 0.5 – 1.5 parts per hundred parts polyol (pphp) water, 10.0 pphp TEGOAMIN33 catalyst, 0.5 – 3.0 pphp sulfated castor oil stabilizer, and 4.0 pphp calcium stearate pore opener [18]. The makeup of the hardener components for the different respective PTK diols was individually optimized to yield scaffolds with mechanical integrity and an intact porous structure. PEUR scaffolds were respectively designated by their polyester precursor as 900t-PEUR, 1000d-PEUR, and 1500t-PEUR and served as hydrolytically-degradable controls. The hardener component elements were first mixed for 30 s at 3300 rpm in a Hauschild DAC 150 FVZ-K SpeedMixer (FlackTek, Inc., Landrum, SC) before adding the HDIt and mixing for an additional 30 s. This reactive liquid mixture was allowed to rise freely for 10-20 min for complete setting and hardening. The targeted index (ratio of NCO to OH equivalents times 100) was 115, where the number of OH equivalents is calculated from the experimentally measured OH number for the relevant PTK diol.

Characterization of Scaffold Physical Properties

The core densities of PTK-UR and PEUR scaffolds were determined by measuring the mass and volume of cylindrical porous scaffold core samples, with the core porosities being subsequently calculated from these density values[18]. The porous morphologies of the different PTK-UR scaffolds were qualitatively assessed by scanning electron microscopy (Hitachi S-4200 SEM, Finchampstead, UK). The amount of unreacted components (sol fraction) in the cross-linked network was measured from the mass loss of dried scaffold cylinders (25 mm × 12 mm) previously incubated in DCM for 24 h.

9

To measure the molecular weight between crosslinks (M_c), scaffold samples (n = 3) were weighed dry and then incubated in DCM for 24 h. After incubation, samples were gently blotted to remove excess DCM and then the samples' swollen mass was measured. These values, along with the solvent parameters, were used in the Flory-Rhener equation to determine M_c. For measuring scaffold hydrophilicity, PTK-UR films of 100%, 50%, and 0% MEE-PTK diols were synthesized using an index of 105 and the gelling catalyst Coscat83 at 1000 ppm. After mixing the catalyst and PTK diol for 30 s at 3300 rpm, HDIt was added and mixed for an additional 30 s. The mixtures were cast into Teflon compression molds and allowed to cure for 18 h at 60°C. The contact angle of water on these PTK-UR films was measured using a Rame-Hart (Mountain Lakes, NJ) Model A-100 contact angle goniometer. A 4 μL water drop was added to the film surface, and after 10 min, an equilibrium contact angle was measured to account for molecular surface reorganization which increased the hydrophilicity at the contact site[53].

Thermal and Mechanical Properties

Thermal transitions were measured by a TA Instruments (New Castle, DE) Q200 DSC and Q800 DMA. For DSC analysis, samples ranging in mass from 10-15 mg were heated from -80° C to 200° C at a rate of 10° C min^{-1}, cooled to -80° C at a rate of -20° C min^{-1}, and heated a second time to 200° C at a rate of 10° C min^{-1}. All transitions were obtained from the second heating run. For dynamic mechanical analysis (DMA, Q800 DMA, TA Instruments, New Castle, DE), cylindrical samples (6 × 6 mm) were analyzed from -80° to 55° C at a ramp rate of 1° C min^{-1}. Scaffolds were compressed at a frequency of 1 Hz with 1% strain during the thermal treatment. Glass transitions were obtained at the peak of tan δ.

The mechanical properties of the different PTK-UR and PEUR scaffold formulations were measured in compression at 37°C in a submersion compression clamp using the Q800 DMA. Cylindrical 6 × 6 mm scaffold samples were tested after incubation in phosphate buffered saline (PBS) for 7 days at 37°C. Using a preload force of 0.1 N, samples were compressed along the longitudinal axis at a strain rate of 10% per min until 60% compressive strain was achieved. The Young's modulus

10

for each sample was calculated from the slope of the initial linear region of each respective stress-strain curve after toe-in.

In Vitro Degradation of PTK-UR and PEUR Scaffolds

Long-term hydrolytic stability of PTK-UR and PEUR scaffolds was determined by incubating 10 mg samples in PBS at 37°C on a shaker and measuring the mass loss at each time point (n = 3). Before beginning the experiment, scaffolds were soaked in an excess of DCM for 24 h to remove any unreacted components before vacuum drying for 24 h. Scaffold samples were removed from the buffer at each time point, rinsed in deionized water, vacuum dried for 48 h, and weighed. The buffer medium was not changed between time points. Short term oxidative degradation rates of PTK-UR scaffolds were similarly assessed using an oxidative degradation medium that simulates *in vivo* oxidative degradation at an accelerated rate[54, 55]. This oxidative medium comprised 20 wt% hydrogen peroxide (H_2O_2) in 0.1 M cobalt chloride ($CoCl_2$), with the H_2O_2 and cobalt ion reacting to stimulate oxidative radical formation [54]. As with the long-term study, triplicate samples were pre-soaked in DCM for 24 h before vacuum drying and incubated at 37°C in the oxidative medium on a shaker. At specified time points over 10 d, samples were removed, rinsed with deionized water, vacuum dried, and weighed. The oxidative medium was replaced every 3 days, and the morphology of both PBS-incubated and H_2O_2-incubated scaffolds was qualitatively assessed with SEM.

The effect of radical concentration on PTK-UR scaffold degradation kinetics was also explored. The original 20% H_2O_2 in 0.1 M $CoCl_2$ degradation medium was diluted ten and one hundred fold to yield a 2% H_2O_2 in 0.01 M $CoCl_2$ solution and a 0.2% H_2O_2 in 0.001 M $CoCl_2$ solution. These three degradation media were used to incubate 100%, 50%, and 0% MEE-PTK-UR scaffolds along with 900t-PEUR control samples, with material preparation steps and incubation conditions being the same as previously described.

Mathematical Modeling of PTK-UR Oxidative Degradation

The degradation behavior of the PTK-UR scaffold formulations were fit to first-order decay kinetics equation to create a mathematical model of scaffold degradation with respect to H_2O_2 concentration. The first-order degradation model is given in **Eq 2**.

$$M_t/M_0 = e^{-kt} \tag{1}$$

In this equation, M_t is the scaffold mass remaining at time t, M_0 is the initial scaffold mass, and k is the degradation rate constant. Non-linear regression was used to fit this first-order degradation model to the experimentally determined degradation data. This method was used to determine the degradation rate constant k for the scaffolds incubated in the different media.

In Vitro Culture of Macrophages on PTK-UR Scaffolds

RAW 264.7 macrophages were cultured in DMEM supplemented with 10% FBS and 1% penicillin/streptomycin. 100% and 0% MEE-PTK-UR scaffolds were cut into 6.5 × 1-mm discs, sterilized by UV-radiation for 1 h (30 min per side), placed into 96-well plates, and incubated with culture medium for 30 min. Macrophages were seeded onto the scaffolds at a density of 2.5×10^5 cells/scaffold. The cells were allowed to adhere to the scaffolds for 3 h, at which point the media were removed and the cells were treated with either fresh culture media or activation media containing 5 μg mL^{-1} lipopolysaccharide (LPS) and 1000 U mL^{-1} interferon gamma (IFN-γ). Cells were incubated on the scaffolds for 3 d with fresh culture media being applied daily. After the 3 d incubation, the scaffolds were fixed in 5% glutaraldehyde for 2 h followed by 2% osmium tetroxide for 1 h. These fixed scaffolds were dehydrated in ascending grades of ethanol before being vacuum dried, sputter-coated, and imaged with SEM to evaluate surface pitting.

Cytotoxicity of PTK-UR and PEUR Scaffolds

NIH 3T3 mouse fibroblasts stably transfected with a firefly luciferase reporter gene were cultured in DMEM supplemented with 10% FBS and 1% penicillin/streptomycin. 100% MEE-PTK-UR, 0% MEE-PTK-UR, and 900t-PEUR scaffolds were cut into 6.5 × 1-mm discs, sterilized by UV-radiation for 1 h (30 min per side), placed into a black-walled 96-well plate, and incubated with culture medium for 30 min. Fibroblasts were seeded at a density of 5.0×10^4 cells/scaffold on n=3 scaffolds and allowed to grow for 0, 1, and 3 days in 200 µL of culture media per well (changed every two days). At the endpoint, the cell-seeded scaffolds were treated with culture media containing a luciferin substrate. After 10 min, the scaffolds were imaged with an IVIS 200 (Xenogen, Alameda, CA) bioluminescence imaging system with an exposure time of 2 min to quantify the luciferase-based bioluminescence signal from each scaffold's viable cell population. All readings were normalized to day 0 bioluminescence values.

In Vivo Degradation of PTK-UR Scaffolds Implanted Subcutaneously in Rats

All surgical procedures were reviewed and approved by Vanderbilt University's Institutional Animal Care and Use Committee. 100% MEE-PTK-UR, 0% MEE-PTK-UR, and 900t-PEUR scaffolds were cut into 10 × 2.5 mm discs, sterilized with ethylene oxide, and implanted into ventral subcutaneous sites in adult male Sprague-Dawley rats. Scaffolds were excised from euthanized animals at weeks 1, 3, 5 and 7 to evaluate new granulation tissue formation in the implants. The excised tissues were fixed in formalin, processed, sectioned, and stained with hematoxylin & eosin. Histological sections were evaluated with Metamorph Imaging Software (Molecular Devices Inc., Sunnyvale CA) to assess wound dimensions and scaffold degradation. The wound area was defined as the cross-sectional area occupied by the scaffold and new tissue growth. Values for the percentage of scaffold area occupying the wound area were normalized to week 1 values to eliminate the effect of scaffold compression over time, and 100% MEE-PTK-UR degradation was fit to the first-order degradation kinetics model seen in Eq. 2.

Statistical Analysis

All data are reported as the mean and standard error of the mean unless otherwise indicated. Statistical analysis was performed using single factor analysis of variance (ANOVA) and Tukey post-hoc comparison tests, with p-values less than 0.05 considered statistically significant.

Results

PTK Polymer Synthesis and Characterization

Thiol-terminated PTK polymers were successfully synthesized from the condensation polymerization of MEE, BDT, and DMP monomers using PTSA as a catalyst (**Figure 2A**). Five copolymers were synthesized with varying percent molar composition of MEE and BDT, and each polymer is designated by its relative mol% MEE. ^{1}H-NMR spectra confirmed that the composition of the synthesized polymers closely matched the monomer ratios in the feed (**Figure 2B, Table 1**), and gel permeation chromatography (GPC) analysis showed that the polymers had M_n values of around 1000 g mol^{-1} with polydispersity index (PDI) values near 1.35 (**Figure S1, Table 1**).

Efficient conversion of terminal thiols to hydroxyls was demonstrated by ATR-FTIR. The thiol absorbance peak at 2550 cm^{-1} was apparent in the thiol-terminated, parent PTKs but did not appear with the hydroxyl-terminated polymers, which generated a characteristic ATR-FTIR hydroxyl peak at 3400 cm^{-1} (**Figure 2C**). OH numbers experimentally measured with titration were utilized to calculate a titration M_n (**Table 1**) that was used to balance the hydroxyl-isocyanate reaction used to form PTK-URs. Consistent with previous findings, the experimental OH numbers trended higher than theoretical values[23].
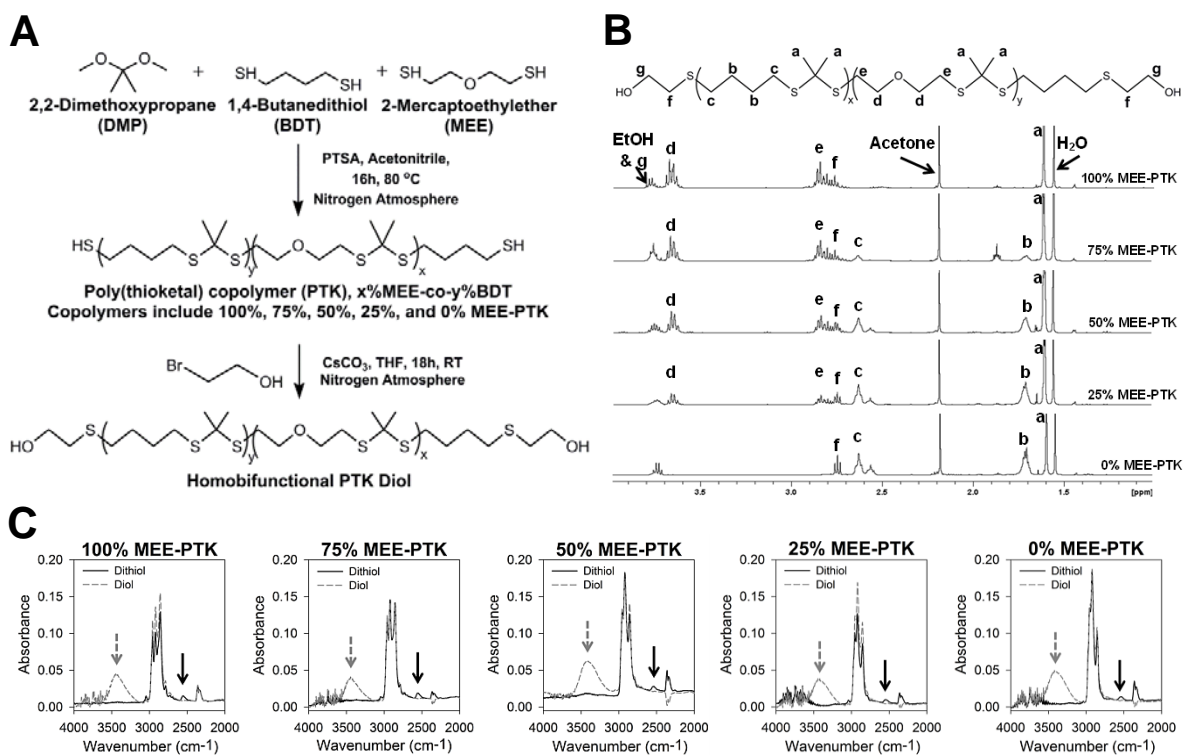
Figure 2. Synthesis and characterization of a family of PTK diols. (A) Scheme for the condensation polymerization of thiol-terminated PTKs and their conversion into PTK diols. (B) ^{1}H-NMR spectra of the PTK copolymer diols. Peaks associated with MEE and BDT monomers correlated with molar composition used in the polymer feed. (C) ATR-FTIR spectra of thiol- and hydroxyl-terminated PTKs. The thiol absorbance peak is seen at 2550 cm^{-1} (black arrow) and the hydroxyl absorbance peak is seen at 3400 cm^{-1} (grey arrow). These spectra demonstrate efficient conversion of PTK terminal thiols into hydroxyls.

Table 1. Characterization of PTK diols.

Copolymer (PTK diol)	Feed MEE%	Actual MEE%[a]	GPC M_n[b]	PDI[b]	Titration M_n[c]
100% MEE-PTK	100%	100%	1027	1.38	825
75% MEE-PTK	75%	76%	1005	1.34	850
50% MEE-PTK	50%	52%	947	1.35	810
25% MEE-PTK	25%	26%	1053	1.36	745
0% MEE-PTK	0%	0%	807	1.32	680

[a]Calculated from NMR peaks at δ=1.72 and δ=3.64 ppm.

[b]Calculated from GPC standards.

[c]Calculated from measured titration OH numbers.

PTK-UR Scaffold Formation and Physical Properties

PTK-UR scaffolds were successfully synthesized from the PTK diols and HDIt, yielding porous, mechanically robust 3D scaffolds (SEM images shown in **Figure S2**). PEUR control scaffolds were also successfully formed from HDIt and the three different polyester prepolymers (1000d, 1500t, and 900t). The resulting PTK-UR and PEUR scaffolds possessed similar sol fraction and porosity, as seen in **Table 2**. The average molecular weight between crosslinks (M_c) for 1000d- and 1500t-PEUR was statistically equal to all of the PTK-UR scaffolds, while the 900t-PEURs had a significantly lower M_c ($p <$ 0.05) relative to all other formulations except for the 100% and 0% MEE-PTK-UR scaffolds (**Table 2**). The relative surface hydrophilicity of the PTK-UR materials was assessed using contact angle measurements on films, with 100%, 50%, and 0% MEE-PTK-URs having contact angle values of 66°, 77°, and 80°, respectively.

Table 2. Physical properties of PTK-UR and PEUR scaffolds.

Scaffold	Sol Fraction (%)	Core Porosity (vol. %)	M_c (kg mol^{-1})
100% MEE PTK-UR	6.9%±1.6%	90.9%±0.4%	7.6±4.2
75% MEE PTK-UR	8.4%±1.4%	89.0%±1.2%	10.1±4.9
50% MEE PTK-UR	9.7%±6.1%	86.9%±1.4%	13.8±6.5
25% MEE PTK-UR	9.1%±2.7%	90.6%±1.5%	9.0±5.0
0% MEE PTK-UR	8.3%±3.2%	88.8%±1.4%	9.0±5.8
900t PEUR	4.1%±1.6%	89.8%±1.2%	2.5±1.6
1500t PEUR	4.7%±0.1%	91.3%±0.2%	13.2±5.4
1000d PEUR	7.7%±0.1%	92.7%±0.7%	7.7±2.8

*All values presented as mean ± standard deviation

Thermal and Mechanical Analysis of PTK-UR Scaffolds

The glass-transition temperature (T_g) of PTK polyols was determined by differential scanning calorimetry (DSC), and the T_g of the PTK-UR scaffolds was measured by DSC and dynamic mechanical analysis (DMA) (**Table S1**). The wet compressive moduli of the PTK-UR scaffolds ranged from 100 - 250 kPa, and the PEUR moduli ranged from 20 – 100 kPa (**Figure 3**). All the PTK-UR formulations had significantly higher modulus values than the 1500t-PEUR and 1000d-PEUR materials, while the lower M_c 900t-PEUR scaffolds possessed stiffness values closer to the PTK-UR samples. However, even this formulation was significantly less stiff than the 100% and 0% MEE-PTK-UR materials.
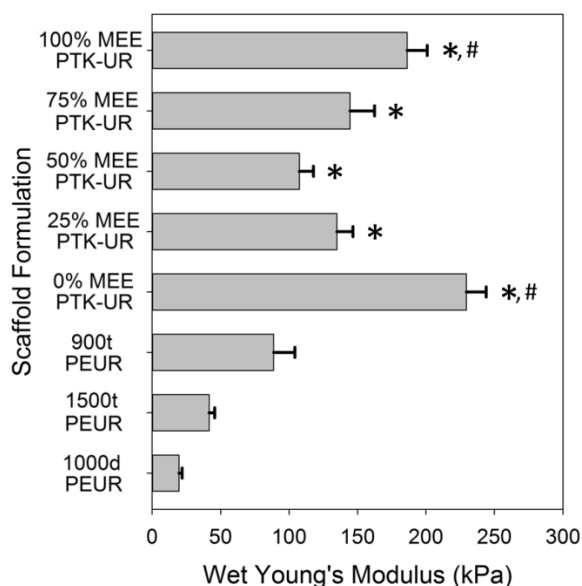
Figure 3. PTK-UR and PEUR scaffold mechanical properties. The compressive moduli of porous scaffolds were determined under fully hydrated conditions at 37°C. *$p < 0.05$ compared to 1500t- and 1000d-PEUR. #$p < 0.05$ compared to 900t-PEUR.

In Vitro **Degradation of PTK-UR Scaffolds under Aqueous and Oxidative Conditions**

The hypothesized oxidative degradation mechanism of PTK copolymers is seen in **Figure 4**. Qualitative PTK-UR degradation was demonstrated by SEM as scaffolds incubated for 10 d in oxidative media illustrated loss of porous architecture and surface pitting, while these morphological changes in scaffold architecture were not apparent following PTK-UR scaffold incubation in PBS for 25 weeks

17

(**Figure 5A and S2**). The PTK-UR scaffolds were stable over a long-term, 25-week study in PBS at 37°C, while the 900t-PEUR scaffolds underwent significant hydrolytic degradation over this time period (**Figure 5B**). Conversely, the PTK-URs rapidly degraded under accelerated oxidative conditions (20% H_2O_2 in 0.1 M $CoCl_2$) as seen in **Figure 5C**. The degradation profiles of all PTK-UR formulations in the 20% H_2O_2 media are seen in **Figure S3**.
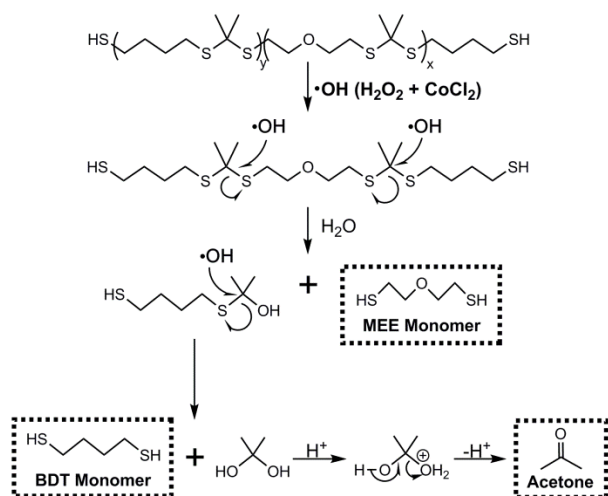
Figure 4. Proposed mechanism for hydroxyl radical degradation of PTK polymers.

Mathematical Model of ROS-Dependent PTK-UR Scaffold Degradation

To further elucidate the relationship between ROS concentration and the degradation rates of the different PTK-UR scaffold formulations, degradation was measured in oxidative media comprising 20%, 2%, and 0.2% H_2O_2 and 0.1, 0.01, and 0.001 M $CoCl_2$, respectively. The degradation rates of PTK-UR scaffolds were dependent on the concentration of H_2O_2 (**Figure 5D-G**). The mass loss profiles of the PTK-UR scaffolds were fit to first-order degradation kinetics (**Eq. 2**) to mathematically model the process of scaffold degradation with respect to H_2O_2 concentration. The model-generated degradation profiles are concurrently shown with the respective experimental data as dotted lines in **Figure 5C-F**, with the derived degradation rate constants being shown in **Figure 5G**. The 900t-PEUR samples incubated in these same oxidative media did not display significant degradation over the same time scale (**Figure 5G and S4**).

18
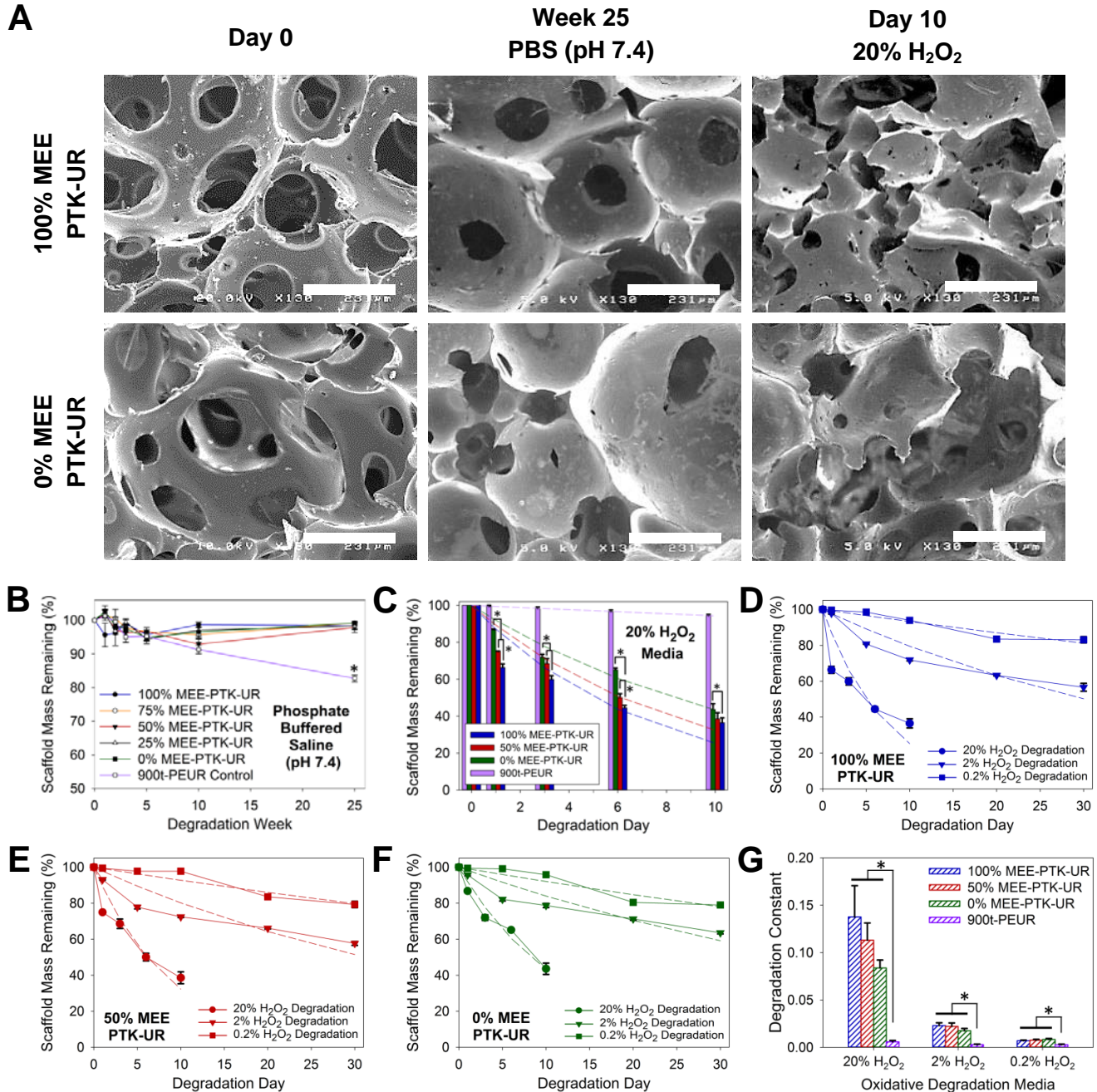
Figure 5. *In vitro* **degradation of PTK-UR scaffolds.** Data are presented as mean ± standard error with n = 3. (A) SEM of PTK-UR scaffolds: freshly made (left column), incubated in PBS for 25 weeks (middle column), and incubated in 20% H_2O_2 media for 10 d (right column). Scale bars = 231 μm. The ROS-degraded scaffolds feature irregular pore morphology and surface pitting. (B) Long-term stability of PTK-UR scaffolds incubated in PBS. (C) Percent degradation of PTK-UR scaffolds incubated in oxidative medium (20% H_2O_2 in 0.1M $CoCl_2$). Dashed lines represent model-generated curves for first-order degradation kinetics, *p < 0.05. Percent mass remaining of (D) 100% MEE-PTK-UR, (E) 50% MEE-PTK-UR, and (F) 0% MEE-PTK-UR scaffolds incubated in oxidative media containing 20%, 2%, and 0.2% H_2O_2. (G) Degradation constants used to generate the best-fit curves in (C-F), as determined by non-linear regression analysis. The PTK-UR but not the PEUR scaffolds exhibited H_2O_2 dose-dependent degradation.

19

In Vitro Cell-Mediated Degradation and Cytocompatibility of PTK-UR Scaffolds

100% and 0% MEE-PTK-UR scaffolds were seeded with murine-derived RAW 267.4 macrophages. Seeded cells were treated with either control culture media or macrophage-activating media containing LPS and IFN-γ. SEM imaging of scaffolds after three days illustrated surface pitting by activated macrophages, but cell mediated scaffold degradation was not apparent for the control cells (**Figure 6A**).

NIH 3T3 mouse fibroblasts stably transduced to express luciferase were seeded onto 100% MEE-PTK-UR, 0% MEE-PTK-UR, and 900t-PEUR scaffolds, and relative cell number was measured based on luciferase activity over 3 days of culture (**Figure 6B**). Cell-generated bioluminescent signal was steadily maintained over the culture period, and there were no significant differences between the scaffold compositions tested.
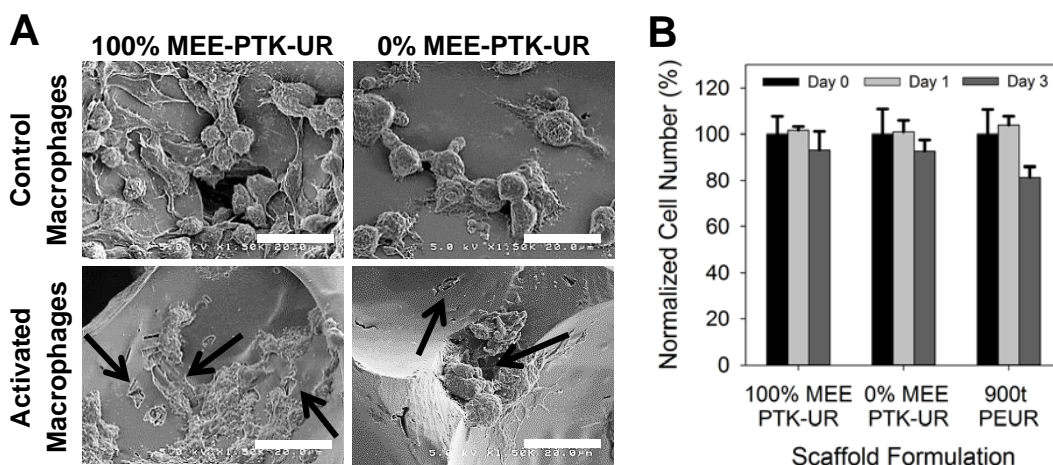
Figure 6. *In vitro* cell-mediated degradation and cytocompatibility of PTK-UR scaffolds. (A) PTK-UR scaffolds seeded with RAW 267.4 macrophages and incubated for 3 d in either control or activation media (LPS and IFN-γ). The activated macrophages generated visible pitting on the scaffold surface (black arrows), indicating ROS-mediated scaffold degradation. Scale bar = 20 μm. (B) In vitro biocompatibility of porous 3D PTK-UR scaffolds. The bioluminescence (cellular viability) from 3T3 fibroblast-seeded scaffolds was normalized to day 0 values and remained stable over 3 d in culture.

***In Vivo* Degradation of PTK-UR Scaffolds in a Rat Subcutaneous Wound Model**

100% MEE-PTK-UR and 900t-PEUR scaffolds subcutaneously implanted into male Sprague-Dawley rats demonstrated robust cellular infiltration, a minimal inflammatory response, and granulation tissue formation by 3 weeks post implantation (**Figure 7A**). The 0% MEE-PTK-UR materials also provoked a minimal inflammatory response from the native tissue but supported visibly less tissue in-growth and were thus not quantitatively analyzed. Both the 100% MEE-PTK-UR and 900t-PEUR materials displayed significant degradation over 7 weeks (**Figure 7B**). However, the 100% MEE-PTK-UR implants followed first-order degradation kinetics (dashed line, **Figure 7B**) and degraded gradually over 7 weeks to reach 40% degradation, whereas at their end point the 900t-PEUR scaffolds were 75% degraded compared to week 1 values, and degradation initialized after week 3. The 900t-PEUR scaffolds were also significantly more compressed than the PTK-UR materials, which stented the implant site significantly more than the PEUR scaffolds (**Figure 7C**). Wound lengths were relatively consistent between PTK-UR and PEUR implant sites over time, while wound area measurements followed trends similar to the scaffold thickness values (**Figures S5 and S6**).
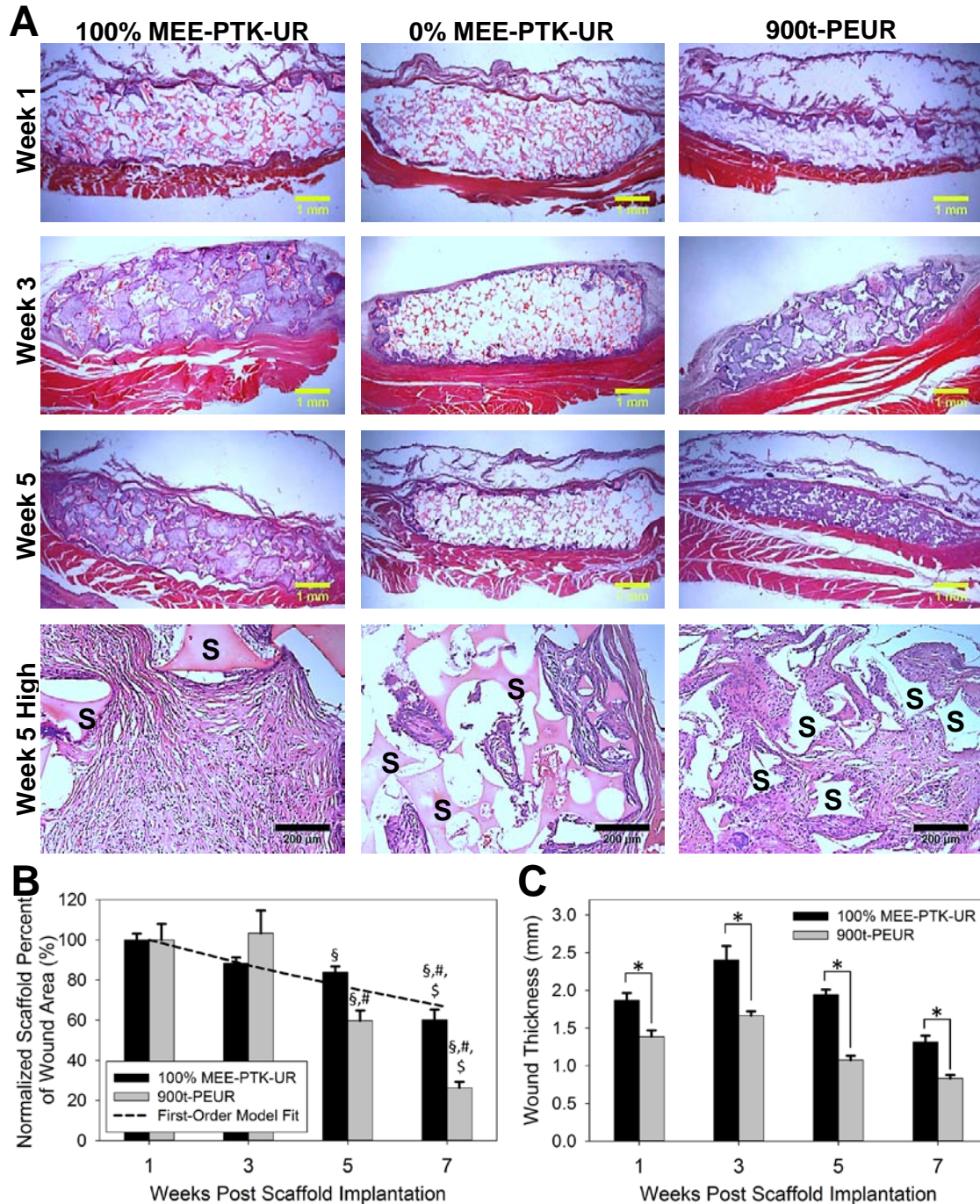
Figure 7. *In vivo* response of subcutaneous PTK-UR scaffolds. (A) Histological illustration of cellular infiltration into PTK-UR and control PEUR scaffolds (designated with *S* in the Week 5 High Magnification panels) in Sprague-Dawley rats. The 0% MEE-PTK-UR formulation did not support new tissue in-growth over 5 weeks. (B) *In vivo* scaffold degradation normalized to week 1. Though initially 90% porous, the PEURs became compressed and experienced rapid late-stage break down in comparison to the slowly degrading PTK-URs which follow first-order degradation kinetics (dashed line represents model-generated curve). $^{§}p < 0.05$ compared to week 1, $^{#}p < 0.05$ compared to week 3, $^{$}p < 0.05$ compared to week 5. (C) Compression of PTK-UR vs. PEUR scaffolds. The PTK-UR scaffolds maintained their mechanical integrity/thickness and provided a greater stenting effect than the PEUR implants, $^{*}p < 0.05$.

Discussion

Many currently utilized tissue engineering scaffolds feature hydrolytically degradable ester bonds that nonspecifically break down in the presence of water. Cleavage of ester bonds produces free carboxylic acids which can acidify the local microenvironment and cause autocatalytic degradation[28], leading to reduced tissue regeneration[30]. Here, a novel PTK-based scaffold technology is presented that is specifically degraded by cell-generated ROS while remaining insensitive to hydrolysis (**Figure 5B**)[44]. Because these PTK-UR materials selectively degrade by cell-mediated activity, they avoid autocatalytic degradation and are anticipated to yield better matched rates of cellular infiltration and scaffold degradation. To this end, PTK copolymers were successfully synthesized with varying chain compositions but similar M_n and PDI values (**Figure 2, Table 1**). The resulting dithiol-terminated MEE-PTK polymers were converted into diols to generate telechelic end groups compatible with standard polyurethane synthesis and to provide PTK polyols amenable to direct comparison with polyesters used in PEUR scaffold formation.

The PTK-UR scaffolds were fabricated using HDIt and compared to PEUR scaffolds made from 900t, 1000d, and 1500t polyester-based PEUR scaffolds. The 900t-PEUR represented a biological control that has been successfully used for *in vivo* applications[24, 56, 57] while the 1000d-PEUR and 1500t-PEUR were synthesized for a more direct material comparison to the PTK-URs because they yield PEUR scaffolds with similar crosslink densities to the PTK-UR scaffolds. The PTK-UR scaffolds produced from the PTK macrodiols were approximately 90% porous and were morphologically similar to more conventional PEUR 3D porous scaffolds. This level of porosity is optimal for promoting cellular in-growth, nutrient exchange, and neo-vascularization in tissue engineering applications[58-60]. The PTK-URs also featured relatively low sol fraction values, indicating that the isocyanates and diols were well matched and efficiently reacted during scaffold formation. As expected, the scaffolds' relative hydrophilicity was influenced by the composition of the PTK polyol, and the contact angle was inversely correlated with the mol% of the more hydrophilic MEE monomer in the PTK copolymer. These data suggest that the 100% MEE-PTK-UR with a contact angle of 66° may be optimal for cellular adhesion

and tissue formation *in vivo*, since more hydrophobic surfaces with contact angles > 76° (such as the 50% and 0% MEE-PTK-UR formulations) preferentially adsorb hydrophobic serum proteins such as albumin over cellular adhesion proteins like fibronectin and vitronectin[61, 62].

Thermal analysis of PTK-UR and PEUR scaffolds, along with their polymeric precursors, indicated that the scaffolds are phase-mixed materials since the 3D materials all possessed a T_g exceeding that of the polyol precursor soft segment[23]. The scaffold T_g values determined by DMA also exceeded those measured by DSC by 30 – 50°C, as has been previously reported for similar 3D PEUR materials[18]. Wet compression testing of these materials indicated that although the 1500t-PEUR, 1000d-PEUR, and PTK-UR scaffolds had similar M_c values (**Table 2**), all of the PTK-UR formulations had significantly higher modulus values than the 1500t-PEUR and 1000d-PEUR materials (**Figure 3**). However, there was no consistent trend between PTK-UR scaffold composition and modulus. Due to its higher crosslink density, the 900t-PEUR achieved stiffness values closer to the PTK-UR samples, though even this formulation was significantly less stiff than the 100% and 0% MEE-PTK-UR materials.

Previous work has demonstrated the selective, ROS-mediated degradation of poly(thioketal) nanoparticles[44]. The PTK-UR scaffolds were formulated with HDIt because it is more oxidatively stable relative to lysing-derived isocyanates[22, 24, 56], allowing more specific study of the degradation behavior of the polyol component. Degradation of PTK-UR and 900t-PEUR scaffolds was tested in an oxidative degradation medium comprising H_2O_2 and $CoCl_2$ that produces hydroxyl radicals[54]. These radicals destabilize the thioketal bond, leading to chain scission and breakdown into the original constitutive monomers (MEE and BDT) and acetone (**Figure 4**). It is predicted that these small byproducts would be rapidly cleared in an *in vivo* environment. Furthermore, these thiolated monomers have been shown to cause limited *in vitro* cytotoxicity[63] and a minimal host inflammatory response *in vivo*[64] when incorporated into a similar polyurethane system.

The long-term stability of PTK-UR scaffolds over 25 weeks in PBS (**Figure 5B**) is significantly different than these materials' rapid degradation under accelerated oxidative conditions as seen in **Figure 5C**, highlighting the ROS-specific degradation mechanism of the PTK-UR scaffolds.

Furthermore, there was a relationship between the PTK composition and degradation rate, as the scaffolds with higher MEE content in the PTK polyol degraded faster (**Figure 5C**). It has been previously reported that ethers are stable in aqueous media but that oxidative radicals can degrade them *in vitro* and *in vivo* [54]. Thus, it is hypothesized that the faster ROS-dependent degradation seen in both the 100% and 50% MEE-PTK-UR materials may result from a combination of oxidative degradation of both thioketals and ethers, while the 0% MEE-PTK-UR scaffolds are degraded solely by thioketal scission. These results indicate that ROS-dependent scaffold degradation rates can be tuned by the composition of the PTK polyol.

For all PTK-UR compositions tested, the degradation rate was dependent on ROS concentrations (**Figure 5D-F**). This dose-dependent relationship between ROS levels and degradation rate coupled with the agreement between the model and experimental data confirm that the PTK-UR scaffolds degrade by first-order kinetics with respect to ROS concentration. The degradation rate constants derived from the non-linear regression fitting of the experimental data gathered in 20% H_2O_2 media (**Figure 5G**) also illustrate the relationship between degradation rate and the %MEE-PTK polyol used in PTK-UR scaffold fabrication, though this trend was decreased under lower H_2O_2 concentrations. In contrast, the 900t-PEUR samples incubated in these same oxidative media did not display H_2O_2 dose-dependent degradation (**Figure 5G and S4**), highlighting the unique degradation mechanism of the PTK-UR relative to PEUR scaffolds. These collective data confirm that PTK-based polyols are selectively cleaved by ROS and that their rate of degradation is first-order with respect to the concentration of radical species in the local environment.

PTK-UR scaffolds were shown to display a high level of *in vitro* cytocompatibility with both RAW 267.4 macrophages and NIH 3T3 fibroblasts. Seeded macrophages were treated with either control culture media or media containing LPS and IFN-γ to activate the macrophages through the classical pathway[65, 66], which is known to lead to ROS production[24, 49]. Scaffolds with activated macrophages displayed enhanced surface pitting while cell-mediated remodeling of the scaffold surface was less evident for the control cells (**Figure 6A**), indicating that the PTK-UR scaffolds were degraded by

physiologically relevant concentrations of ROS. Further highlighting these materials' cytocompatibility, luciferase-expressing fibroblasts seeded on PTK-UR and PEUR scaffolds steadily maintained their bioluminescent signal over the culture period (**Figure 6B**), similar to cell growth profiles seen in other biocompatible 3D scaffolds[67, 68]. Similar cell lines stably transduced to express luciferase have been previously used to reliably measure *in vitro* cytocompatibility, as their constitutive luciferase activity directly correlates with cell number[31]. Furthermore, none of the scaffold formulations displayed a significant difference in bioluminescence over time or relative to each other, indicating that PTK-UR scaffolds possessed biocompatibility levels analogous to PEUR scaffolds that are cytocompatible and have been successfully utilized *in vivo*[24].

This *in vivo* cytocompatibility was confirmed by histological analysis of subcutaneous implants, which showed that neither the 100% nor 0% MEE-PTK-UR formulations elicited an inflammatory response from the native tissue that was obviously different from the conventional PEUR scaffolds (**Figure 7A**). However, the 0% MEE-PTK-UR scaffolds supported much less robust tissue infiltration into the scaffold interior relative to the 100% MEE-PTK-UR or 900t-PEUR scaffolds. One possible explanation for this result is that the relative hydrophobicity of the 0% MEE-PTK-UR scaffolds (80° contact angle) did not allow cells to properly adhere and migrate into the scaffold interior. As a result, only the 100% MEE-PTK-UR and 900t-PEUR histology samples were quantitatively analyzed. Both these formulations supported new tissue growth into the scaffold interior 3 weeks after implantation and displayed significant biodegradation over 7 weeks (**Figure 7B**). The 900t-PEURs experienced a steep increase in degradation after 3 weeks as expected from previous work with these materials[24], while the 100% MEE-PTK-UR scaffolds displayed first-order degradation over time. This finding confirms the initial hypothesis that PTK-UR scaffolds degrade by a cell-mediated mechanism compared to hydrolytic degradation of more conventional PEUR materials, which have been recently shown to undergo to autocatalytic degradation *in vivo* resulting in a reduced wound healing response[30]. Furthermore, the PTK-UR samples were more mechanically resilient and were more effective in maintaining implant geometry as seen in **Figure 7A and C**. Though all scaffolds initially possessed 90% porosity and were

cut to the same dimensions pre-implantation, the PEUR materials were significantly more compressed than the PTK-UR scaffolds by week 1. As the wound length was relatively consistent between PTK-UR and PEUR scaffolds (**Figure S5**), the total wound area values closely mirrored the trends seen in the scaffold thickness measurements (**Figure S6**). This *in vivo* compression of PEUR scaffolds can be potentially attributed to both the significantly higher modulus of the 100% MEE-PTK-UR samples relative to the 900t-PEUR formulation (**Figure 3**), and also to the 900t-PEUR T_g value (34.4 °C) which is close to body temperature (**Table S1**). This relatively high T_g predicts a less mechanically resilient PEUR scaffold at body temperature because it would be in its glassy transition viscoelastic region. The stenting effect seen in these PTK-UR scaffolds is advantageous because it ensures that the scaffold pores remain open, maximizing cell infiltration and new tissue formation and potentially decreasing scarring in clinical applications [69].

Conclusions

ROS are key mediators of cell function in both health and disease, especially at sites of inflammation and tissue healing. Utilizing these cell-generated species as triggers for selective polymer degradation represents a promising methodology for creating a tissue engineering scaffolds with well-matched rates of tissue in-growth and cell-mediated scaffold degradation. Here, novel poly(thioketal) polymers featuring tunable chain compositions and ROS-mediated degradation rates have been developed towards this end. These PTK polymers were successfully incorporated into 3D porous tissue engineering scaffolds, generating materials with more robust mechanical properties than similar constructs fabricated from standard polyesters. These PTK-UR scaffolds were selectively degraded by ROS but were stable under aqueous conditions, indicating that their biodegradation would be exclusively cell-mediated as opposed to PEURs that hydrolytically degrade independent of cellular activity. Moreover, the *in vitro* oxidative degradation rates of the PTK-URs followed first-order degradation kinetics and displayed dose-dependent degradation with respect to ROS levels. PTK scaffolds exhibited cytocompatibility *in vitro* and were shown to be degraded by activated ROS-

secreting macrophages. The PTK-UR scaffolds also supported cell infiltration and granulation tissue formation *in vivo*, and their superior mechanical properties lead to significantly greater stenting of subcutaneous implants compared to more standard PEUR scaffolds. Furthermore, the PTK-URs experienced controlled first-order *in vivo* biodegradation in contrast to the PEUR scaffolds which experienced dramatic increases in degradation at later time points. These collective data indicate that PTK-URs represent a useful new class of biomaterials that provide a robust, cell-degradable substrate for guiding new tissue formation.

CHAPTER III

ONGOING AND FUTURE WORK

Confirming *In Vivo* ROS-Dependent Scaffold Degradation

As demonstrated in Chapter II, PTK-UR scaffolds display first order degradation kinetics both *in vitro* and *in vivo*. It was also clearly demonstrated that increased levels of ROS increased the degradation rate *in vitro*, though this behavior has not been confirmed in an *in vivo* setting. To further confirm the ROS-dependent nature of PTK-UR degradation, scaffolds will be implanted into streptozotocin (STZ)-induced diabetic rats for a 7 week time course. Oxidative stress and heightened ROS levels are hallmark pathogenic outcomes of diabetes[70, 71], thus making an STZ-induced rat model ideal for studying the effects of ROS-mediated PTK-UR degradation. It is predicted that PTK-UR constructs will more quickly in a diabetic model than in the previously shown non-diabetic rats due to the higher *in vivo* ROS concentrations. Though higher oxidative stress has been clearly demonstrated in diabetic rodent models in previous work, ROS levels in the tissues of the sacrificed rats will also be quantitatively measured with ROS-responsive fluorescent[72] or luminescent probes[42] to directly tie heightened ROS with accelerated PTK-UR scaffold degradation. Tissue sections can also be processed for immunohistochemical staining with antibodies targeting macrophages, as these cells are known to be prime mediators of ROS production[49]. These studies will help confirm the ROS-dependent PTK-UR degradation mechanism and will further elucidate the potential *in vivo* performance of these novel materials.

Critically Sized Bone Defect Model

Though PTK-UR scaffolds have demonstrated *in vivo* biocompatibility and the capacity to effectively regenerate soft tissue, they have not been applied for the regeneration of bone defects (the intended clinical application). To this end, PTK-UR scaffolds will be doped with decellularized allograft

bone particles as described in previous work[25, 50] to increase the mechanical stiffness of the constructs to more appropriately match the scaffold mechanical properties with that of native bone. Furthermore, these scaffold composites will be loaded with recombinant human bone morphogenetic protein-2 (rhBMP-2) as this growth factor is an essential component in promoting new bone growth[25]. *In vitro* testing of scaffold composites' mechanical properties, degradation kinetics, biocompatibility, and rhBMP-2 release will all be performed prior to *in vivo* testing. Upon validation of proper scaffold composite *in vitro* performance, these materials with and without loaded rhBMP-2 will be placed in critically sized calvarial defects in rabbits to evaluate their ability to regenerate bone tissue over 12 weeks.

Adaptation to Other Applications

These novel materials have demonstrated the ability to achieve specific, ROS-mediated degradation both *in vitro* and *in vivo*. Most biodegradable materials used in regenerative medicine applications achieve degradation by incorporating hydrolytically-degradable ester bonds or protease-degradable peptides into the polymer structure. As previously discussed in Chapter I, ester bond hydrolysis is non-specific and can lead to mismatches between scaffold degradation rates and tissue ingrowth while synthetic peptides are difficult to create on the scale needed for most tissue engineering applications. Thus, PTK polymers could be incorporated into many different regenerative medicine scaffolds for an alternative strategy to confer biodegradability to a material. In particular, thiol-terminated PTK polymers could be incorporated into covalently cross-linked poly(ethylene glycol) (PEG) hydrogels by reacting the PTK thiol groups with maleimide units attached to a multi-arm PEG macromer[73]. This approach would generate a new class of cell-degradable hydrogels amenable to cell delivery and regeneration of soft tissues.

REFERENCES

1. Bohner M. Resorbable biomaterials as bone graft substitutes. *Materials Today*. 2010;13:24-30

2. Ahlmann E, Patzakis M, Roidis N, Shepherd L, Holtom P. Comparison of anterior and posterior iliac crest bone grafts in terms of harvest-site morbidity and functional outcomes. *The Journal of Bone & Joint Surgery*. 2002;84:716-720

3. Ooms EM, Wolke JGC, van de Heuvel MT, Jeschke B, Jansen JA. Histological evaluation of the bone response to calcium phosphate cement implanted in cortical bone. *Biomaterials*. 2003;24:989-1000

4. Mitchell W, Bridget Matthews J, Stone MH, Fisher J, Ingham E. Comparison of the response of human peripheral blood mononuclear cells to challenge with particles of three bone cements in vitro. *Biomaterials*. 2003;24:737-748

5. Hollinger JO, Battistone GC. Biodegradable bone repair materials synthetic polymers and ceramics. *Clinical Orthopaedics and Related Research*. 1986;207:290

6. Whang K, Thomas CH, Healy KE, Nuber G. A novel method to fabricate bioabsorbable scaffolds. *Polymer*. 1995;36:837-842

7. Ishaug-Riley SL, Crane-Kruger GM, Yaszemski MJ, Mikos AG. Three-dimensional culture of rat calvarial osteoblasts in porous biodegradable polymers. *Biomaterials*. 1998;19:1405-1412

8. Lowry KJ, Hamson KR, Bear L, Peng YB, Calaluce R, Evans ML, Anglen JO, Allen WC. Polycaprolactone/glass bioabsorbable implant in a rabbit humerus fracture model. *Journal of Biomedical Materials Research*. 1997;36:536-541

9. Ciapetti G, Ambrosio L, Savarino L, Granchi D, Cenni E, Baldini N, Pagani S, Guizzardi S, Causa F, Giunti A. Osteoblast growth and function in porous poly ε-caprolactone matrices for bone repair: A preliminary study. *Biomaterials*. 2003;24:3815-3824

10. Leong KW, Simonte V, Langer RS. Synthesis of polyanhydrides: Melt-polycondensation, dehydrochlorination, and dehydrative coupling. *Macromolecules*. 1987;20:705-712

11. Ibim SEM, Uhrich KE, Attawia M, Shastri VR, El-Amin SF, Bronson R, Langer R, Laurencin CT. Preliminary in vivo report on the osteocompatibility of poly(anhydride-co-imides) evaluated in a tibial model. *Journal of Biomedical Materials Research*. 1998;43:374-379

12. Nilsson A, Liljensten E, Bergström C, Sollerman C. Results from a degradable tmc joint spacer (artelon) compared with tendon arthroplasty. *The Journal of Hand Surgery*. 2005;30:380-389

13. Gogolewski S, Gorna K, Turner AS. Regeneration of bicortical defects in the iliac crest of estrogen-deficient sheep, using new biodegradable polyurethane bone graft substitutes. *Journal of Biomedical Materials Research Part A*. 2006;77A:802-810

14. Lü J-M, Wang X, Marin-Muller C, Wang H, Lin PH, Yao Q, Chen C. Current advances in research and clinical applications of plga-based nanotechnology. *Expert Review of Molecular Diagnostics*. 2009;9:325-341

15. Bezwada RS, Jamiolkowski DD, Lee I-Y, Agarwal V, Persivale J, Trenka-Benthin S, Erneta M, Suryadevara J, Yang A, Liu S. Monocryl® suture, a new ultra-pliable absorbable monofilament suture. *Biomaterials*. 1995;16:1141-1148

16. Dang W, Daviau T, Brem H. Morphological characterization of polyanhydride biodegradable implant gliadel® during in vitro and in vivo erosion using scanning electron microscopy. *Pharm Res*. 1996;13:683-691

17. Chen J, Xu J, Wang A, Zheng M. Scaffolds for tendon and ligament repair: Review of the efficacy of commercial products. *Expert Review of Medical Devices*. 2009;6:61-73

18. Hafeman AE, Li B, Yoshii T, Zienkiewicz K, Davidson JM, Guelcher SA. Injectable biodegradable polyurethane scaffolds with release of platelet-derived growth factor for tissue repair and regeneration. *Pharm Res*. 2008;25:2387-2399

19. Ignatius AA, Claes LE. In vitro biocompatibility of bioresorbable polymers: Poly(l, dl-lactide) and poly(l-lactide-co-glycolide). *Biomaterials*. 1996;17:831-839

20. Hua N, Sun J. Body distribution of poly(d,l-lactide-co-glycolide) copolymer degradation products in rats. *J Mater Sci: Mater Med*. 2008;19:3243-3248

21. Visscher GE, Robison RL, Maulding HV, Fong JW, Pearson JE, Argentieri GJ. Biodegradation of and tissue reaction to 50:50 poly(dl-lactide-co-glycolide) microcapsules. *Journal of Biomedical Materials Research*. 1985;19:349-365

22. Guelcher SA. Biodegradable polyurethanes: Synthesis and applications in regenerative medicine. *Tissue Engineering: Part B*. 2008;14:3-17

23. Guelcher SA, Srinivasan A, Hafeman A, Gallagher KM, Doctor JS, Khetan S, McBride S, Hollinger JO. Synthesis, in vitro degradation, and mechanical properties of two-component poly(ester urethane)urea scaffolds: Effects of water and polyol composition *Tissue Engineering*. 2007;13:2321-2333

24. Hafeman AE, Zienkiewicz KJ, Zachman AL, Sung H-J, Nanney LB, Davidson JM, Guelcher SA. Characterization of the degradation mechanisms of lysine-derived aliphatic poly(ester urethane) scaffolds. *Biomaterials*. 2011;32:419-429

25. Dumas JE, BrownBaer PB, Prieto EM, Guda T, Hale RG, Wenke JC, Guelcher SA. Injectable reactive biocomposites for bone healing in critical-size rabbit calvarial defects. *Biomedical Materials*. 2012;7:024112

26. Fu K, Pack DW, Klibanov AM, Langer R. Visual evidence of acidic environment within degrading poly(lactic-co-glycolic acid) (plga) microspheres. *Pharm Res*. 2000;17:100-106

27. Lu L, Peter SJ, D. Lyman M, Lai H-L, Leite SM, Tamada JA, Uyama S, Vacanti JP, Langer RS, Mikos AG. In vitro and in vivo degradation of porous poly(dl-lactic-co-glycolic acid) foams. *Biomaterials*. 2000;21:1837-1845

28. Antheunis H, van der Meer J-C, de Geus M, Heise A, Koning CE. Autocatalytic equation describing the change in molecular weight during hydrolytic degradation of aliphatic polyesters. *Biomacromolecules*. 2010;11:1118-1124

29. An YH, Woolf SK, Friedman RJ. Pre-clinical in vivo evaluation of orthopaedic bioabsorbable devices. *Biomaterials*. 2000;21:2635-2652

30.   Dumas JE, Prieto EM, Zienkiewicz KJ, Guda T, Wenke JC, Bible JE, Holt GE, Guelcher SA. Balancing the rates of new bone formation and polymer degradation enhances healing of weight-bearing allograft/polyurethane composites in rabbit femoral defects. *Tissue Engineering Part A*. 2013

31.   Li H, Yu SS, Miteva M, Nelson CE, Werfel T, Giorgio TD, Duvall CL. Matrix metalloproteinase responsive, proximity-activated polymeric nanoparticles for sirna delivery. *Advanced Functional Materials*. 2013;23:3040-3052

32.   Ku T-H, Chien M-P, Thompson MP, Sinkovits RS, Olson NH, Baker TS, Gianneschi NC. Controlling and switching the morphology of micellar nanoparticles with enzymes. *Journal of the American Chemical Society*. 2011;133:8392-8395

33.   West JL, Hubbell JA. Polymeric biomaterials with degradation sites for proteases involved in cell migration. *Macromolecules*. 1998;32:241-244

34.   Lutolf MP, Weber FE, Schmoekel HG, Schense JC, Kohler T, Muller R, Hubbell JA. Repair of bone defects using synthetic mimetics of collagenous extracellular matrices. *Nat Biotech*. 2003;21:513-518

35.   Dey J, Xu H, Shen J, Thevenot P, Gondi SR, Nguyen KT, Sumerlin BS, Tang L, Yang J. Development of biodegradable crosslinked urethane-doped polyester elastomers. *Biomaterials*. 2008;29:4637-4649

36.   Stakleff KS, Lin F, Smith Callahan LA, Wade MB, Esterle A, Miller J, Graham M, Becker ML. Resorbable, amino acid-based poly(ester urea)s crosslinked with osteogenic growth peptide with enhanced mechanical properties and bioactivity. *Acta Biomaterialia*. 2013;9:5132-5142

37.   Patterson J, Hubbell JA. Enhanced proteolytic degradation of molecularly engineered peg hydrogels in response to mmp-1 and mmp-2. *Biomaterials*. 2010;31:7836-7845

38.   Parrott MC, Luft JC, Byrne JD, Fain JH, Napier ME, DeSimone JM. Tunable bifunctional silyl ether cross-linkers for the design of acid-sensitive biomaterials. *Journal of the American Chemical Society*. 2010;132:17928-17932

39. Thayer AM. Improving peptides. *Chemical & Engineering News*. 2011;89:13-20

40. Hensley K, Robinson KA, Gabbita SP, Salsman S, Floyd RA. Reactive oxygen species, cell signaling, and cell injury. *Free Radical Biology and Medicine*. 2000;28:1456-1462

41. Pacher P, Beckman JS, Liaudet L. Nitric oxide and peroxynitrite in health and disease. *Physiological Reviews*. 2007;87:315-424

42. Liu WF, Ma M, Bratlie KM, Dang TT, Langer R, Anderson DG. Real-time in vivo detection of biomaterial-induced reactive oxygen species. *Biomaterials*. 2011;32:1796-1801

43. Napoli A, Valentini M, Tirelli N, Muller M, Hubbell JA. Oxidation-responsive polymeric vesicles. *Nat Mater*. 2004;3:183-189

44. Wilson DS, Dalmasso G, Wang L, Sitaraman SV, Merlin D, Murthy N. Orally delivered thioketal nanoparticles loaded with tnf-α–sirna target inflammation and inhibit gene expression in the intestines. *Nat Mater*. 2010;9:923-928

45. de Gracia Lux C, Joshi-Barr S, Nguyen T, Mahmoud E, Schopf E, Fomina N, Almutairi A. Biocompatible polymeric nanoparticles degrade and release cargo in response to biologically relevant levels of hydrogen peroxide. *Journal of the American Chemical Society*. 2012;134:15758-15764

46. Gupta MK, Meyer TA, Nelson CE, Duvall CL. Poly(ps-b-dma) micelles for reactive oxygen species triggered drug release. *Journal of Controlled Release*. 2012;162:591-598

47. Broaders KE, Grandhe S, Fréchet JMJ. A biocompatible oxidation-triggered carrier polymer with potential in therapeutics. *Journal of the American Chemical Society*. 2010;133:756-758

48. Shim MS, Xia Y. A reactive oxygen species (ros)-responsive polymer for safe, efficient, and targeted gene delivery in cancer cells. *Angewandte Chemie International Edition*. 2013;52:6926-6929

49. Yu SS, Koblin RL, Zachman AL, Perrien DS, Hofmeister LH, Giorgio TD, Sung H-J. Physiologically relevant oxidative degradation of oligo(proline) cross-linked polymeric scaffolds. *Biomacromolecules*. 2011;12:4357-4366

50. Dumas JE, Zienkiewicz K, Tanner SA, Prieto EM, Bhattacharyya S, Guelcher SA. Synthesis and characterization of an injectable allograft bone/polymer composite bone void filler with tunable mechanical properties. *Tissue Engineering, Part A: Tissue Engineering*. 2010;16:2505-2518

51. Salvatore RN, Smith RA, Nischwitz AK, Gavin T. A mild and highly convenient chemoselective alkylation of thiols using cs2co3–tbai. *Tetrahedron Letters*. 2005;46:8931-8935

52. ASTM-International. E1899 - 08. Standard test method for hydroxyl groups using reaction with p-toluenesulfonyl isocyanate (tsi) and potentiometric titration with tetrabutylammonium hydroxide. 2008.

53. Pike JK, Ho T, Wynne KJ. Water-induced surface rearrangements of poly(dimethylsiloxane−urea−urethane) segmented block copolymers. *Chemistry of Materials*. 1996;8:856-860

54. Schubert MA, Wiggins MJ, Anderson JM, Hiltner A. Role of oxygen in biodegradation of poly(etherurethane urea) elastomers. *Journal of Biomedical Materials Research*. 1997;34:519-530

55. Christenson EM, Anderson JM, Hiltner A. Oxidative mechanisms of poly(carbonate urethane) and poly(ether urethane) biodegradation: In vivo and in vitro correlations. *Journal of Biomedical Materials Research Part A*. 2004;70A:245-255

56. Adolph EJ, Hafeman AE, Davidson JM, Nanney LB, Guelcher SA. Injectable polyurethane composite scaffolds delay wound contraction and support cellular infiltration and remodeling in rat excisional wounds. *Journal of Biomedical Materials Research Part A*. 2012;100A:450-461

57. Page JM, Prieto EM, Dumas JE, Zienkiewicz KJ, Wenke JC, Brown-Baer P, Guelcher SA. Biocompatibility and chemical reaction kinetics of injectable, settable polyurethane/allograft bone biocomposites. *Acta Biomaterialia*. 2012;8:4405-4416

58. Hu Y, Grainger DW, Winn SR, Hollinger JO. Fabrication of poly(α-hydroxy acid) foam scaffolds using multiple solvent systems. *Journal of Biomedical Materials Research*. 2002;59:563-572

59.   Karageorgiou V, Kaplan D. Porosity of 3d biomaterial scaffolds and osteogenesis. *Biomaterials*. 2005;26:5474-5491

60.   Mikos AG, Temenoff JS. Formation of highly porous biodegradable scaffolds for tissue engineering. *Electronic Journal of Biotechnology*. 2000;3:114-119

61.   Harbers GM, Grainger DW. Cell-material interactions: Fundamental design issues for tissue engineering and clinical considerations. In: Guelcher SA, Hollinger JO, eds. *An introduction to biomaterials*. CRC Press, Taylor & Francic Group; 2006.

62.   Arima Y, Iwata H. Effect of wettability and surface functional groups on protein adsorption and cell adhesion using well-defined mixed self-assembled monolayers. *Biomaterials*. 2007;28:3074-3082

63.   Eglin D, Griffon S, Alini M. Thiol-containing degradable poly(thiourethane-urethane)s for tissue engineering. *Journal of Biomaterials Science, Polymer Edition*. 2010;21:477-491

64.   Laschke MW, Strohe A, Scheuer C, Eglin D, Verrier S, Alini M, Pohlemann T, Menger MD. In vivo biocompatibility and vascularization of biodegradable porous polyurethane scaffolds for tissue engineering. *Acta Biomaterialia*. 2009;5:1991-2001

65.   Aste-Amezaga M, Ma X, Sartori A, Trinchieri G. Molecular mechanisms of the induction of il-12 and its inhibition by il-10. *The Journal of Immunology*. 1998;160:5936-5944

66.   Jayakumar A, Widenmaier R, Ma X, McDowell MA. Transcriptional inhibition of interleukin-12 promoter activity in leishmania spp.–infected macrophages. *Journal of Parasitology*. 2008;94:84-93

67.   Oh SH, Ward CL, Atala A, Yoo JJ, Harrison BS. Oxygen generating scaffolds for enhancing engineered tissue survival. *Biomaterials*. 2009;30:757-762

68.   Rockwood DN, Akins Jr RE, Parrag IC, Woodhouse KA, Rabolt JF. Culture on electrospun polyurethane scaffolds decreases atrial natriuretic peptide expression by cardiomyocytes in vitro. *Biomaterials*. 2008;29:4783-4791

69.   Lee SY, Oh JH, Kim JC, Kim YH, Kim SH, Choi JW. In vivo conjunctival reconstruction using modified plga grafts for decreased scar formation and contraction. *Biomaterials.* 2003;24:5049-5059

70.   Hamada Y, Kitazawa S, Kitazawa R, Fujii H, Kasuga M, Fukagawa M. Histomorphometric analysis of diabetic osteopenia in streptozotocin-induced diabetic mice: A possible role of oxidative stress. *Bone.* 2007;40:1408-1414

71.   Hamada Y, Fujii H, Kitazawa R, Yodoi J, Kitazawa S, Fukagawa M. Thioredoxin-1 overexpression in transgenic mice attenuates streptozotocin-induced diabetic osteopenia: A novel role of oxidative stress and therapeutic implications. *Bone.* 2009;44:936-941

72.   Selvam S, Kundu K, Templeman KL, Murthy N, García AJ. Minimally invasive, longitudinal monitoring of biomaterial-associated inflammation by fluorescence imaging. *Biomaterials.* 2011;32:7785-7792

73.   Phelps EA, Enemchukwu NO, Fiore VF, Sy JC, Murthy N, Sulchek TA, Barker TH, García AJ. Maleimide cross-linked bioactive peg hydrogel exhibits improved reaction kinetics and cross-linking for cell encapsulation and in situ delivery. *Advanced Materials.* 2012;24:64-70
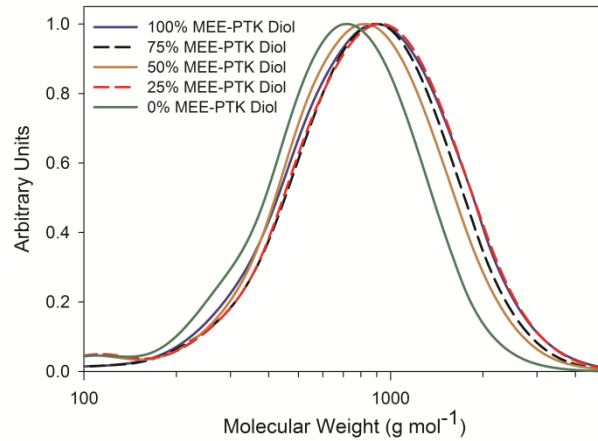
APPENDIX

Appendix A: Supplementary Figures

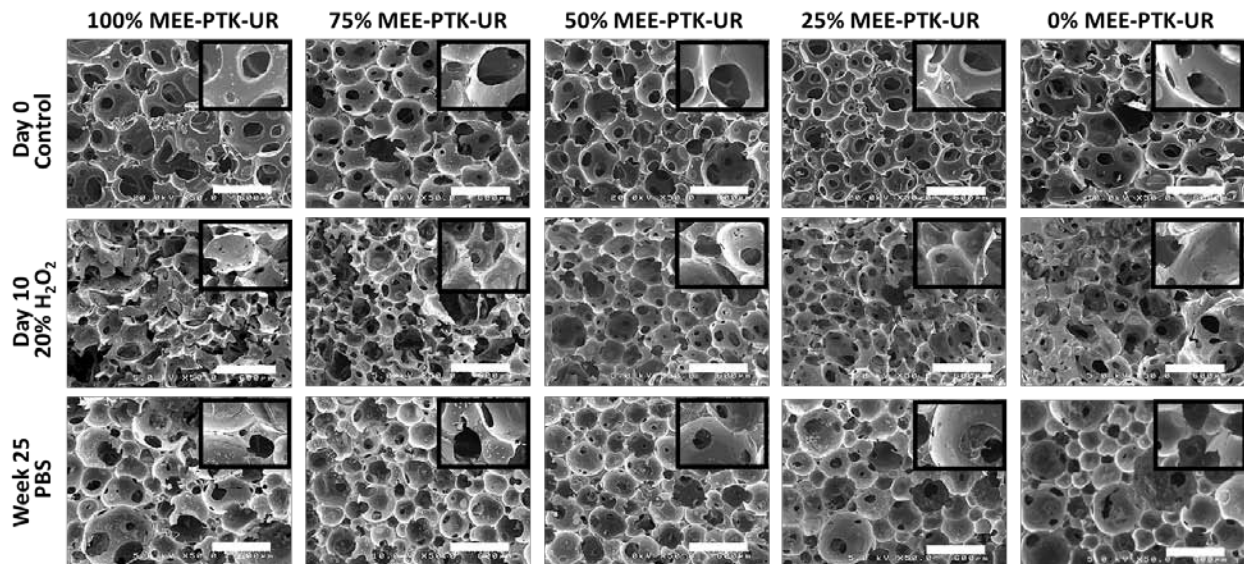**Figure S1. GPC chromatograms of PTK diols.**

Figure S2. SEM images of PTK-UR scaffolds. Day 0 samples (top row) show representative untreated scaffolds. The day 10 degradation samples (middle row) were incubated in 20% H_2O_2 in 0.1M $CoCl_2$ for 10 d at 37°C to demonstrate oxidative degradation of the PTK-URs (note visible changes in structure of "macro-pores" and appearance of "micro-pores" in the struts of the scaffold). Week 25 PBS samples (bottom row) were incubated in PBS for 25 weeks at 37°C to demonstrate the resistance of the PTKs to hydrolytic breakdown. White scale bar represents 600 μm, and the inset images display higher magnification views (2.6x magnification of large image).

Table S1. Thermomechanical properties of PTK-UR and PEUR scaffolds and neat polymers.

	Polymer	Scaffold	
	DSC T_g (°C)	DSC T_g (°C)	DMA T_g (°C)
100% MEE-PTK	-66.1	-25.2	20.7
75% MEE-PTK	-67.7	-36.0	14.9
50% MEE-PTK	-78.5	-11.1	13.9
25% MEE-PTK	-72.9	-27.9	20.3
0% MEE-PTK	-76.8	-19.3	23.1
900 Triol Polyester	-47.7	-1.7	34.4
1500 Triol Polyester	-56.9	-26.4	24.7
1000 Diol Polyester	-43.1	-30.1	18.2
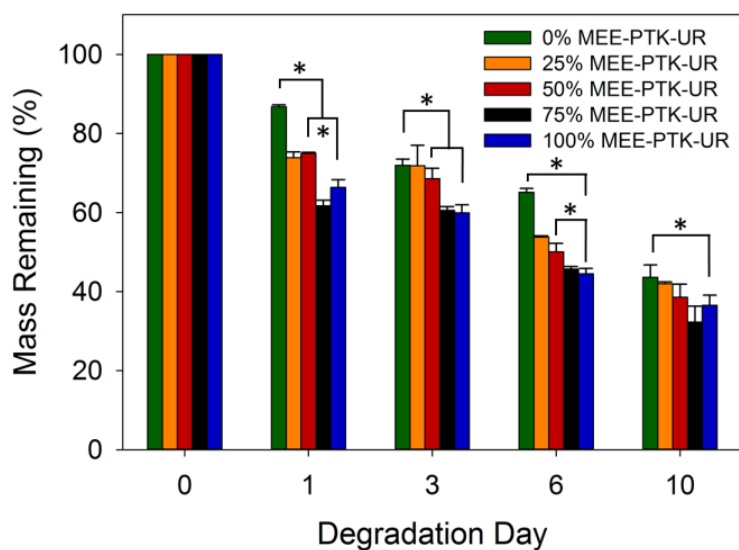
Figure S3. *In vitro* oxidative degradation of the full set of PTK-UR scaffolds. Scaffolds were incubated in accelerated oxidative conditions (20% H_2O_2 in 0.1M $CoCl_2$). For simplicity, only 100%, 50%, and 0% MEE-PTK-UR samples were displayed with statistical comparisons (*$p < 0.05$).
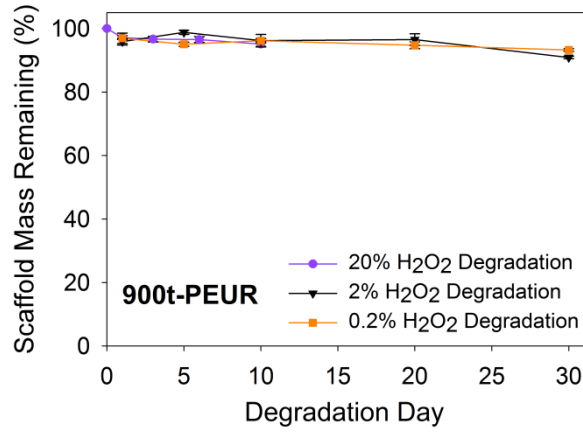
Figure S4. H$_2$O$_2$ dose-dependent degradation of 900t-PEUR scaffolds.
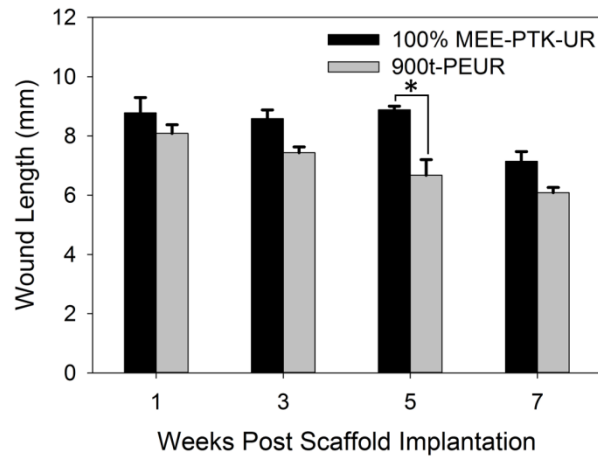

Figure S5. Subcutaneous wound lengths of implanted 100% MEE-PTK-UR and 900t-PEUR scaffolds. Implanted for 7 weeks, *p < 0.05.
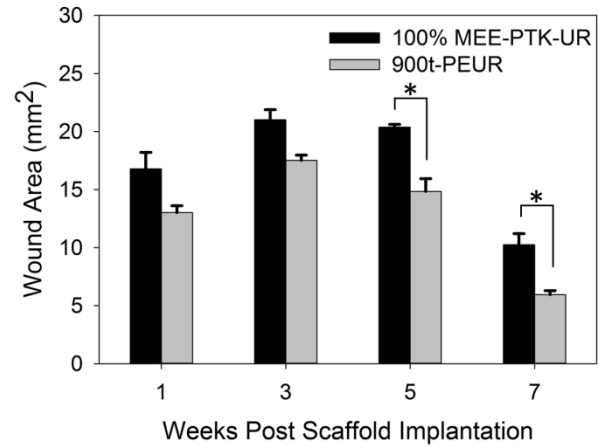

Figure S6. Subcutaneous wound areas of implanted 100% MEE-PTK-UR and 900t-PEUR scaffolds. Implanted for 7 weeks, *p < 0.05.